

***Ab Initio* Simulations of Dense Helium Plasmas**

Cong Wang,¹ Xian-Tu He,^{1,2} and Ping Zhang^{1,2,*}

¹*LCP, Institute of Applied Physics and Computational Mathematics,*

P.O. Box 8009, Beijing 100088, People's Republic of China

²*Center for Applied Physics and Technology,*

Peking University, Beijing 100871, People's Republic of China

Abstract

We study the thermophysical properties of dense helium plasmas by using quantum molecular dynamics and orbital-free molecular dynamics simulations, where densities are considered from 400 to 800 g/cm³ and temperatures up to 800 eV. Results are presented for the equation of state. From the Kubo-Greenwood formula, we derive the electrical conductivity and electronic thermal conductivity. In particular, with the increase in temperature, we discuss the change in the Lorenz number, which indicates a transition from strong coupling and degenerate state to moderate coupling and partial degeneracy regime for dense helium.

PACS numbers: 51.30.+i, 52.25.Fi, 52.27.Gr, 52.65.Yy

*Corresponding author: zhang_ping@iapcm.ac.cn

Pressure induced physical properties of hot dense helium plasmas are of crucial interest for inertial confinement fusion (ICF) and astrophysics [1–3]. Complete burning of deuterium-tritium (DT) capsule follows the fusion reaction $D+T \rightarrow n+He+17.6\text{MeV}$, thus accurate knowledge of the equation of states (EOS) and the relative transport coefficients for helium are essential in typical ICF designs. In the direct-drive scheme, thermal transports in ICF plasmas play a central role in predicting laser absorption [4], shock timing [5], and Rayleigh-Taylor instabilities grown at the fuel-ablator interface or at the hot spot-fuel interface [6–8], while in the indirect-drive ICF, the efficiency of the x-ray conversion is also determined by thermal conduction [9]. Accurate modeling of electrical conductivity is important for precisely determining interactions between electrons and plasmas, because high-energy electron beam has been considered to be the most suitable source for igniting the hot spot much smaller than the dense DT core in the fast ignitor [10]. Because of these important items mentioned above, the EOS and electronic transport properties for hot dense helium are highly recommended to be presented and understood. From the theoretical point of view, various assumptions have been used to predict the electrical conductivity and electronic thermal conductivity for weakly coupled and strongly degenerated plasmas [11–14]. These classic methods widely disagree at high density and are incorrect to model nonlinear screening caused by electronic polarization. Quantum molecular dynamic (QMD) simulation [15, 16], which is free of adjustable parameters or empirical interionic potentials, has been proven to be ideally suited for studying warm dense matter. However, large number of occupied electronic states and overlap between pseudocores limit the use of this method at high temperatures and high densities.

In the present work, direct QMD simulations based on plane-wave density functional theory (DFT) have been adopted to study helium at both high temperatures and high densities, along the 400 to 800 g/cm³ isochore and temperatures up to 800 eV. The EOS data have been determined for a wide range of densities and temperatures. We apply Kubo-Greenwood formula as a starting point for the evaluation of the dynamic conductivity $\sigma(\omega)$ from which the dc conductivity (σ_{dc}) and electronic thermal conductivity (K) can be extracted.

We introduce the *ab initio* plane-wave code ABINIT [17–19] to perform QMD simulations. A series of volume-fixed supercells including N atoms, which are repeated periodically throughout the space, form the elements of our calculations. After Born-Oppenheimer

approximation, electrons are quantum mechanically treated through plane-wave, finite-temperature DFT, where the electronic states are populated according to Fermi-Dirac distributions. The exchange-correlation functional is determined by local density approximation (LDA) with Teter-Pade parametrization [20], and the temperature dependence of exchange-correlation functional, which is convinced to be as small as negligible, is not taken into account. The selection of pseudopotential approximations, which separate core electrons from valence electrons, prevents general QMD simulations from high-density region with the convenience of saving computational cost. Because of the density-induced overlap of the pseudopotential cutoff radius and delocalization of core electrons, this frozen-core approximation only works at moderate densities. As a consequence, a Coulombic pseudopotential with a cutoff radius $r_s = 0.001$ a.u., which is used to model dense helium up to 800 g/cm^3 , has been built to overcome the limitations. The plane-wave cutoff energy is set to 200.0 a.u., because large basis set is necessary in modelling wavefunctions near the core. Sufficient occupational band numbers are included in the overall calculations (the occupation down to 10^{-6} for electronic states are considered). Γ point and $3 \times 3 \times 3$ Monkhorst-Pack scheme \mathbf{k} points are used to sample the Brillouin zone in molecular dynamics simulations and electronic structure calculations, respectively, because EOS (transport coefficients) can only be modified within 5% (15%) for the selection of higher number of \mathbf{k} points. A total number of 64 helium atoms are used in the cubic box. Isokinetic ensemble is adopted in present simulations, and local equilibrium is kept through setting the electronic (T_e) and ionic (T_i) temperatures to be equal. Each dynamics simulation is lasted for 6000 steps, and the time steps for the integrations of atomic motion are selected according to different densities (temperatures) [21]. Then, EOS is averaged over the subsequent 1000 step simulations.

QMD simulations have only been run for temperatures up to 300 eV, for higher temperatures, the thermal excited electronic states increase dramatically, and are currently numerically intractable. For temperatures between 10 eV and 1000 eV, the EOS of dense helium are also obtained from orbital-free molecular dynamic (OFMD) simulations for comparison with the QMD results. In this scheme, orbital-free functional is derived from the semi-classical development of the Mermin functional [22], which leads to the finite-temperature Thomas-Fermi expression for the kinetic part. OFMD simulations are numerically available for temperatures up to 1000 eV, where QMD simulations became prohibitive. The electronic

density, which is the only variable in OFMD simulations, is Fourier transformed during the calculation, and numerical convergence in terms of the mesh size has been insured for all the simulations.

Two nondimensional parameters are used to characterize the state of plasmas, namely, the ion-ion coupling and the electron degeneracy parameters. The former one is commonly defined as $\Gamma_{ii} = Z^{*2}/(k_B T a)$, which describes the ratio of the mean electrostatic potential energy and the mean kinetic energy of the ions. Here, Z^* is the average ionization degree, which is equal to 2 in the present system and a is the ionic sphere radius. The degeneracy parameter $\theta = T/T_F$ is the ratio of the temperature to the Fermi temperature $T_F = (3/\pi^2 n_e)^{2/3}/3$. Both of the parameters are summarized in Table I for the studied densities and temperatures.

TABLE I: Ion-ion coupling parameter (Γ_{ii}) and electron degeneracy parameter θ .

| ρ (g/cm ³) | 400 | | 480 | | 600 | | 800 | |
|-----------------------------|---------------|----------|---------------|----------|---------------|----------|---------------|----------|
| T (eV) | Γ_{ii} | θ | Γ_{ii} | θ | Γ_{ii} | θ | Γ_{ii} | θ |
| 10 | 28.85 | 0.02 | 30.66 | 0.02 | 33.03 | 0.01 | 36.35 | 0.01 |
| 20 | 14.43 | 0.04 | 15.33 | 0.03 | 16.51 | 0.03 | 18.18 | 0.02 |
| 50 | 5.77 | 0.09 | 6.13 | 0.08 | 6.61 | 0.07 | 7.27 | 0.06 |
| 100 | 2.89 | 0.18 | 3.07 | 0.16 | 3.30 | 0.14 | 3.64 | 0.11 |
| 200 | 1.44 | 0.36 | 1.53 | 0.32 | 1.65 | 0.27 | 1.82 | 0.22 |
| 300 | 0.96 | 0.54 | 1.02 | 0.47 | 1.10 | 0.41 | 1.21 | 0.34 |
| 400 | 0.72 | 0.71 | 0.77 | 0.63 | 0.83 | 0.54 | 0.91 | 0.45 |
| 500 | 0.58 | 0.89 | 0.61 | 0.79 | 0.66 | 0.68 | 0.73 | 0.56 |
| 800 | 0.36 | 1.43 | 0.38 | 1.26 | 0.41 | 1.09 | 0.45 | 0.90 |

The accurate determination of the transport coefficients depends on a precise description of the EOS. The wide-range EOS are obtained from both quantum and semiclassical molecular dynamic simulations. As have been shown in Table I, our simulations start from strongly coupled and highly degenerate states, then reach moderate coupling and partial degeneracy states. To examine our results, we also calculate the EOS of hydrogen along 80 g/cm³ isochore up to 1000 eV, and the data are in accordance with previous theoretical predictions [23, 24], as shown in Fig. 1. Good agreements are also shown between our QMD

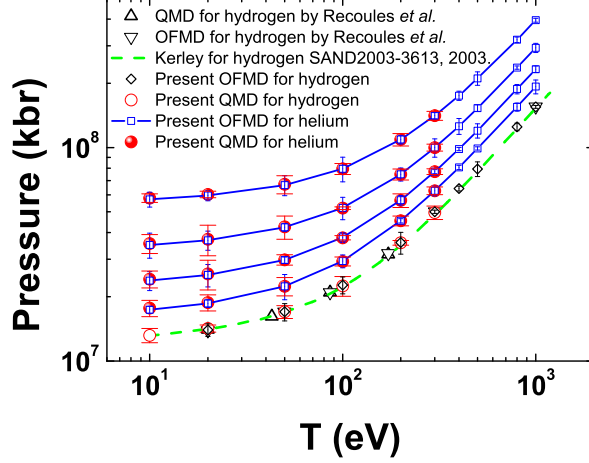


FIG. 1: (Color online) Calculated EOS (pressure versus temperature) for dense helium. The QMD and OFMD results, where the error bars are shown by using wide and narrow caps, are labelled as red filled circles and blue open squares, respectively. Previous theoretical predictions obtained by Recoules *et al.* (up and down triangles) [23] and Kerley (green dashed line) [24], where the EOS of dense hydrogen along the 80 g/cm³ isochore, are also shown for comparison.

and OFMD results, due to the ideal metallization of helium in the hot dense regime. The simulated EOS along temperature for dense helium shows systematic behavior, and smooth functions ($P = \sum A_{ij} \rho^i T^j$), which can be simply used in hydrodynamic simulations for hot dense helium and astrophysical applications, have been constructed (coefficients A_{ij} have been listed in Table II).

TABLE II: Pressure (kbar) expansion coefficients A_{ij} in terms of density (g/cm³) and temperature (eV).

| i | A_{i0} | A_{i1} | A_{i2} |
|-----|----------|----------|----------|
| 0 | 26.77 | 2710.10 | -7.02 |
| 1 | 10819.04 | 398.98 | 0.08 |
| 2 | 69.92 | -0.07 | 0.00 |

The linear response of hot dense helium to external electrical field and temperature gradient can be characterized by the electrical and heat current densities. The key to evaluate these linear-response transport properties is the kinetic coefficients based on the

Kubo-Greenwood formula

$$\hat{\sigma}(\epsilon) = \frac{1}{\Omega} \sum_{k,k'} |\langle \psi_k | \hat{v} | \psi_{k'} \rangle|^2 \delta(\epsilon_k - \epsilon_{k'} - \epsilon), \quad (1)$$

where $\langle \psi_k | \hat{v} | \psi_{k'} \rangle$ are the velocity matrix elements, Ω is the volume of the supercell, and ϵ_k are the electronic eigenvalues. The kinetic coefficients \mathcal{L}_{ij} in the Chester-Thellung version [25] are given by

$$\mathcal{L}_{ij} = (-1)^{i+j} \int d\epsilon \hat{\sigma}(\epsilon) (\epsilon - \mu)^{(i+j-2)} \left(-\frac{\partial f(\epsilon)}{\partial \epsilon} \right), \quad (2)$$

with μ being the chemical potential and $f(\epsilon)$ the Fermi-Dirac distribution function. We obtain the electrical conductivity σ

$$\sigma = \mathcal{L}_{11}, \quad (3)$$

and electronic thermal conductivity K is

$$K = \frac{1}{T} (\mathcal{L}_{22} - \frac{\mathcal{L}_{12}^2}{\mathcal{L}_{11}}), \quad (4)$$

where T is the temperature. Eqs. (3) and (4) are energy-dependent, then the electrical conductivity and electronic thermal conductivity are obtained through extrapolating to zero energy. Those formulation are implemented in the ABINIT code, and have lead to good results for liquid aluminum [26] and hot dense hydrogen [23], where Troullier-Martins potential and Coulombic potential were used respectively. Within the framework of finite-temperature DFT, chemical potential is evaluated through fitting the set of occupation numbers corresponding to the set of eigenvalues with the usual functional form for the Fermi-Dirac distribution. The δ function in Eq. 1 is broaden in the calculations by a Gaussian function, which has been tested to obtain smooth curves.

The Lorentz number L is defined as

$$L = \frac{K}{\sigma T} = \gamma \frac{e^2}{k_B^2}. \quad (5)$$

The rule of force responsible for the electronic scattering characterizes γ . From the Wiedemann-Franz law, γ is $\pi^2/3$ and L is 2.44×10^{-8} in the degenerate regime (low temperature). For the nondegenerate case (high temperature), γ is 1.5966 and L is 1.18×10^{-8} . No classical assumptions are available for γ value in the intermediate region. As a consequence, the electronic thermal conductivity can not be deduced from the electrical conductivity by using Wiedemann-Franz law. Direct predictions of electrical and thermal conductivity from QMD simulations are then rather interesting.

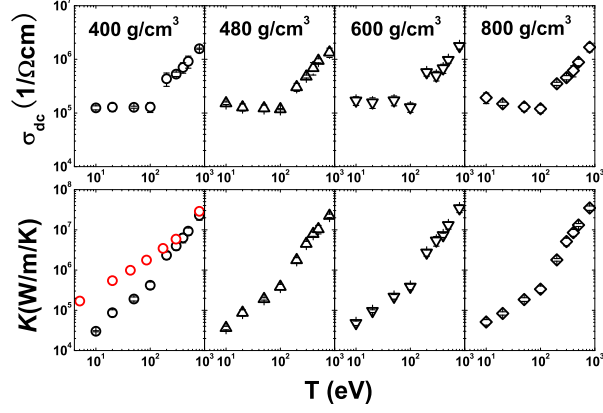


FIG. 2: (Color online) Calculated electrical conductivity (upper panels) and electronic thermal conductivity (lower panels) as functions of temperature at four densities of 400, 480, 600, and 800 g/cm³. For comparison, electronic thermal conductivity for dense hydrogen is also shown as red open circles.

In order to get converged transport coefficients, ten independent snapshots, which are selected during one molecular dynamics simulation at given conditions, are picked up to calculate electrical conductivity and electronic thermal conductivity as running averages. For temperatures below 300 eV, atomic configurations are directly extracted from QMD simulations, while they are taken from OFMD simulations for higher temperatures. Let us stress here that, one-body electronic states are populated according to a Fermi-Dirac distribution in QMD simulations, and a large number of occupied orbitals are introduced at high temperatures. Thus this method is rather time consuming.

In Fig. 2 we plot the electrical conductivity and electronic thermal conductivity as functions of temperature. While at relatively low temperatures up to 100 eV the electrical conductivity changes slowly, it turns to smoothly increase at higher temperatures. The electronic thermal conductivity shows a sustaining increase with temperature, as in Fig. 2 (lower panel). As temperatures arise from 10 to 800 eV, electronic thermal conductivity is of great importance in ICF applications, where these thermodynamic conditions are encountered in the pellet target fusion. In general ICF designs, several models are used to evaluate thermal conductivity, such as Hubbard and Lee-More models [12, 14]. Previous theoretical predictions for dense hydrogen have demonstrated that the electronic thermal conductivity obtained by QMD simulations are in fairly good agreement with the Hubbard

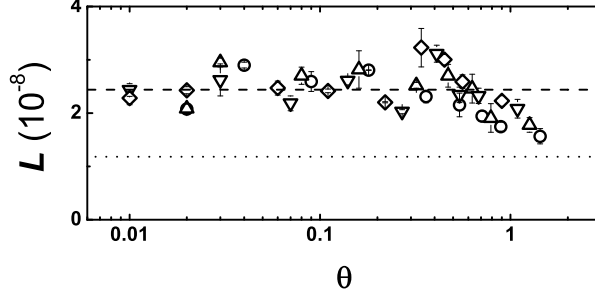


FIG. 3: Lorenz number as a function of electron degeneracy parameter. To distinguish different densities, open circle, up triangle, down triangle, and open diamond are used to denote densities of 400, 480, 600, 800 g/cm³, respectively. The relative degeneracy parameter can be read from Table. I. The dashed line is the value of the degenerate limit, and the dotted line is the value of nondegenerate case.

model. For very high temperatures, the results for Lee-More model merge into the Spitzer thermal conductivity [11], which are accordant with QMD simulations [23]. As a comparison, we also plot the thermal conductivity for dense hydrogen in Fig. 2. It is indicated that at temperatures below 200 eV, electronic thermal conductivity for hydrogen plasma is larger than that of helium. However, they tend to merge with each other for higher temperatures.

Using the calculated electrical and thermal conductivity, the Lorentz ratio is extracted and shown in Fig. 3. In the strong coupling and degenerate region, the computed Lorentz number vibrates around ideal value of 2.44×10^{-8} , which is predicted by the nearly free electron model. This model is valid in the case where Born approximation is applicable because scattering of the electrons by the ions is sufficiently weak. With the increase of temperature, where dense helium enters moderate coupling and a partial degeneracy regime, Lorenz number tends to decrease and approach to the nondegenerate value of 1.18×10^{-8} .

In summary, we have performed *ab initio* QMD simulations to study the thermophysical properties of dense helium plasmas under extreme conditions as reached in ICF experiments. As a result, highly converged EOS data (pressures up to 10^8 kbar), for which Coulombic potential with a very small cutoff radius is adopted to model ultra-dense helium, have been obtained. We have constructed smooth functions to fit the QMD data for the pressure, which is applicable for astrophysics and ICF designs. Using Kubo-Greenwood formula, the electrical conductivity and electronic thermal conductivity have been systematically

determined and carefully discussed. The examination of Lorenz number, as well as that of the calculated plasmas parameters (Table I), has indicated a gradual transition from a strong coupling and degenerate state to a moderate coupling and partial degeneracy regime for dense helium. We expect the present simulated results provide a guiding line in the practical ICF hydrodynamical simulations with the helium plasma participated.

This work was supported by NSFC under Grants No. 11005012 and No. 51071032, by the National Basic Security Research Program of China, and by the National High-Tech ICF Committee of China.

-
- [1] S. Atzeni and J. Meyer-ter-Vehn, *The Physics of Inertial Fusion: Beam Plasma Interaction, Hydrodynamics, Hot Dense Matter*, International Series of Monographs on Physics (Clarendon Press, Oxford, 2004).
 - [2] J. D. Lindl, *Inertial Confinement Fusion: The Quest for Ignition and Energy Gain Using Indirect Drive*, (Springer- Verlag, New York, 1998).
 - [3] J. Nuckolls *et al.*, Nature (London) **239** 139 (1972).
 - [4] W. Seka *et al.*, Phys. Plasmas **15** 056312 (2008).
 - [5] T. R. Boehly *et al.*, Phys. Plasmas **13** 056303 (2006).
 - [6] H. Azechi *et al.*, Phys. Plasmas **4** 4079 (1997).
 - [7] S. G. Glendinning *et al.*, Phys. Rev. Lett. **78** 3318 (1997).
 - [8] V. Lobatchev *et al.*, Phys. Rev. Lett. **85** 4522 (2000).
 - [9] J. D. Lindl *et al.*, Phys. Plasmas **11** 339 (2004).
 - [10] H. Cai *et al.*, Phys. Rev. Lett. **102** 245001 (2009).
 - [11] L. Spitzer *et al.*, Phys. Rev. **89** 977 (1953).
 - [12] W. B. Hubbard *et al.*, Astrophys. J. **146** 858 (1966).
 - [13] H. Brysk *et al.*, Plasma Phys. **17** 473 (1975).
 - [14] Y. T. Lee *et al.*, Phys. Fluids **27** 1273 (1984).
 - [15] A. Kietzmann *et al.*, Phys. Rev. Lett. **101** 070401 (2008).
 - [16] W. Lorenzen *et al.*, Phys. Rev. Lett. **102** 115701 (2009).
 - [17] The ABINIT code, which is a common project of the Université Catholique de Louvain, Corning Incorporated, Commissariat à l’Energie Atomique, Université de Liège, Mitsubishi

Chemical Corp. and other contributions, is available at <http://www.abinit.org>.

- [18] X. Gonze *et al.*, Comput. Mater. Sci. **25** 478 (2002).
- [19] F. Bottin *et al.*, Comput. Mater. Sci. **42** 329 (2008).
- [20] S. Goedecker *et al.*, Phys. Rev. B **54** 1703 (1996).
- [21] The time steps have been taken as $\Delta t = a/20\sqrt{k_B T/m_{He}}$, where $a = (3/4\pi n_i)^{1/3}$ is the ionic sphere radius (n_i is the ionic number density), $k_B T$ presents the kinetic energy, and m_{He} is the ionic mass. A few hundred of plasma periods are included in this choice of simulations.
- [22] M. Brack and R. K. Bhaduri, *Semiclassical Physics* (Westview Press, Boulder, CO, 2003), ISBN 0813340845.
- [23] V. Recoules, *et al.*, Phys. Rev. Lett. **102** 075002 (2009).
- [24] G. I. Kerley, Sandia National Laboratory Tech. Rep. SAND2003-3613, 2003.
- [25] G.V. Chester and A. Thellung, Proc. Phys. Soc. (London) **77**, 1005 (1961).
- [26] V. Recoules, *et al.*, Phys. Rev. B **72** 104202 (2005).